Hindawi Publishing Corporation
Journal of Nanomaterials
Volume 2015, Article ID 796895, 5 pages
http://dx.doi.org/10.1155/2015/796895

Research Article

Surface Nanostructure Formations in an AISI 316L Stainless Steel Induced by Pulsed Electron Beam Treatment

Yang Cai, Kemin Zhang, Zhimin Zhang, Jiawei Dong, Yuan Lei, and Tao Zhang

School of Materials Engineering, Shanghai University of Engineering Science, Shanghai 201620, China

Correspondence should be addressed to Kemin Zhang; zhangkm@sues.edu.cn

Received 18 October 2014; Accepted 13 November 2014

Academic Editor: Gang Ji

Copyright © 2015 Yang Cai et al. This is an open access article distributed under the Creative Commons Attribution License, which permits unrestricted use, distribution, and reproduction in any medium, provided the original work is properly cited.

High current pulsed electron beam (HCPEB) is an efficient technique for surface modifications of metallic materials. In the present work, the formations of surface nanostructures in an AISI 316L stainless steel induced by direct HCPEB treatment and HCPEB alloying have been investigated. After HCPEB Ti alloying, the sample surface contained a mixture of the ferrite and austenite phases with an average grain size of about 90 nm, because the addition of Ti favors the formation of ferrite. In contrast, electron backscattered diffraction (EBSD) analyses revealed no structural refinement on the direct HCPEB treated sample. However, transmission electron microscope (TEM) observations showed that fine cells having an average size of 150 nm without misorientations, as well as nanosized carbide particles, were formed in the surface layer after the direct HCPEB treatment. The formation of nanostructures in the 316L stainless steel is therefore attributed to the rapid solidification and the generation of different phases other than the steel substrate in the melted layer.

1. Introduction

AISI 316L stainless steel, referred to as 316L SS hereafter, is widely used in the biomedical field for producing various implants or surgery tools. The good resistance to general corrosion and high biocompatibility in human body of the 316L SS are essential advantages for its biomedical applications. However, 316L SS is still prone to unexpected pitting or localized corrosion in the complex physical environment [1–3], leading to the failure of implants or Ni release that may do harm to human organs. Considering that corrosion occurs in the near surface region, it is thus efficient to modify the microstructure and composition in the surface layer of 316L SS so that the corrosion performance of the steel can be improved instead of changing the bulk [4].

In recent years, intense-pulsed energetic beams, such as ion, electron, and laser beams, are emerging as new surface treatment techniques for improving the surface properties of various materials [5–13]. These pulsed energetic beams allow high density energy to be introduced into the very top surface layer of the target materials within a very short duration. Among these pulsed beam techniques, the high current pulsed electron beam (HCPEB) technique is developed fairly recently for surface modifications of metallic materials [8]. The pulsed electron beam has its own advantages over ion and laser beams. The electron beam has a deep penetration depth in metals, and it introduces pure energy into the surface layer without severe contaminations. Such pulsed electron beam irradiation induces rapid heating, melting, and possible evaporating followed by rapid solidification and cooling of the surface layers [14]. The temperature rising inducing thermal stresses and crater eruption associated shock waves may generate plastic deformations in the top surface layer and the subsurface layers far beyond the heat affected zone [15]. As a result, improved surface properties of the target material, often unachievable through conventional surface treatment techniques, can be obtained fairly easily [10, 11]. It has been shown that ultrafine/nanostructures can be generated in local regions on the surface of some materials after the HCPEB treatment [5, 9]. However, the conditions needed for the formation of nanostructures in the HCPEB treated surface layer are still not known yet.

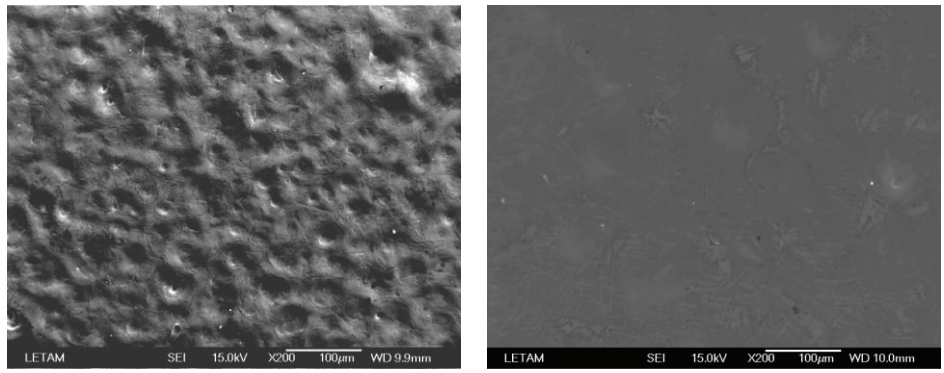

(a) (b)

Figure 1: Typical SEM images taken on the HCPEB Ti alloyed (a) and direct treated (b) samples.

In the present work, the formation of surface nanostructures in the 316L SS subjected to the direct HCPEB treatment and HCPEB Ti alloying is investigated comparatively. The main purpose is to understand the mechanism associated with the formation of surface nanostructures induced by HCPEB treatments, which is of great importance for designing new strategies to improve surface properties of materials.

2. Experimental

2.1. Samples Preparation. The material chosen in this work is an austenitic AISI 316L stainless steel. The steel bar was solution-treated at 1100°C for half an hour followed by water quenching. The initial material has an average grain size of 35 μm. Samples for HCPEB treatment were discs of 12 mm in diameter and 2 mm in thickness. They were ground with sand papers and polished with diamond paste of 1 μm. The sample surfaces were ultrasonically cleaned in acetone. For HCPEB alloying treatments, a thick Ti powder layer, about 350 micrometers, was precoated on the sample surface by brushing. The particle size of the Ti power is about 70~80 μm.

2.2. HCPEB Treatment. The surface treatment of 316L SS samples was conducted with a Nadezhda-2 type HCPEB source. The electron pulses are generated by an explosive emission graphite cathode. The accelerating voltage, magnetic fields intensity, and anode-collector distance control the beam energy density. More details about the HCPEB system can be found in [5, 6]. The electron beam treatment parameters are set as follows: energy density ~3 J/cm^2 and pulse duration ~1.5 μs; the dwell time between each pulse was 10 s with the number of pulses being 20 for both alloying and direct treatments.

2.3. Characterization. A JEOL 6500F type field emission gun scanning electron microscope (FEG-SEM) equipped with an electron backscattered diffraction (EBSD) attachment was used to gain information about the microstructure and phase formed on the treated 316L SS samples. For EBSD analyses, the SEM was operated at 15 kV with the sample tilted by 70°. Conventional X-ray diffraction (θ-2θ mode) was carried out using a SHIMADZU XRD-6000 apparatus equipped with a Cu-K_α radiation source to analyze the phase state at the sample surface. A Philips CM20 transmission electron microscope (TEM) is used to characterize the microstructures in the surface layer of the treated stainless steel samples.

3. Results and Discussions

3.1. Surface Morphology and Phase Components. Figures 1(a) and 1(b) show the typical SEM images taken on the samples induced by HCPEB alloying and direct HCPEB treatment, respectively. Figure 1(a) shows the surface morphology of the Ti alloyed sample after 20 pulses of HCPEB treatment. It is seen that high density of craters formed on the surface after the HCPEB treatment. The crater formation is usually related to the eruption of inclusions in the surface layer during the HCPEB treatment, which leads to the surface purification of the target materials [14]. The crater formation also favors the composition homogenization in the surface layer as the second phases particles or large inclusions can be spread in a scale around 100 μm [9]. Figure 1(b) shows the typical SEM image on the surface of the direct HCPEB treated sample. Apparently, the surface is smoother and the density of craters on the surface is much lower as compared with that on the Ti alloyed sample, which can be attributed to the repeated melting and cleaning of surface layer from inclusions [14]. However, for the Ti alloyed sample, the precoated Ti layer needs to be melted prior to the melting of the substrate; thus the purification effect from the electron beam on the substrate layer is weakened due to less energy input on the substrate. As a result, more craters are present on the Ti alloyed sample than on the direct HCPEB treated sample.

The phases present in the surface layer of the direct HCPEB treated and Ti alloyed samples were identified by using XRD. The results are given in Figure 2. For the direct HCPEB treated 316L SS sample, no phase transformation occurs and all the diffraction peaks can be identified as the austenite γ-Fe phase. For the Ti alloyed sample, the indexation of the XRD pattern reveals that two phases,

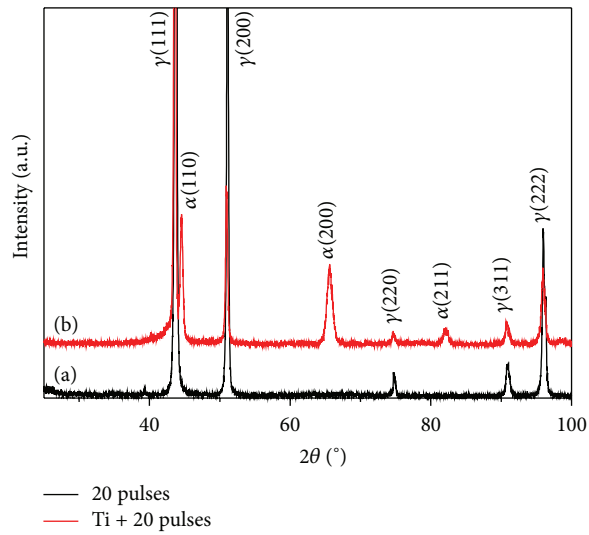

FIGURE 2: XRD patterns of the direct HCPEB treated (a) and Ti alloyed (b) samples.

α-Fe and γ-Fe phases, formed in the surface layer. It is known from Fe-Ti phase diagram that Ti favors the formation of α-Fe phase in Fe [16]. During the HCPEB treatment, the Ti powder precoated on 316L SS was melted and dissolved into the substrate and resolidified to form α-Fe phase in the Ti rich regions.

3.2. Formation of Surface Nanostructures. Figure 3 shows the EBSD orientation map taken on the direct HCPEB treated sample. The average grain size on the surface is determined to be 32 μm, which is only slightly smaller than the size of untreated material, indicating that no significant grain refinement occurs after the HCPEB treatment. Figure 4(a) shows the typical TEM image in the top surface layer of the direct HCPEB treated sample. It is clearly seen that cells having size of about 100–150 nm and clear boundaries are present in the surface layer. A careful look at the image reveals also very fine particles, having size of several nm, which locate mainly at cell boundaries, as arrowed in Figure 4(a). Based on previous investigations on mould steels and high speed steels [9, 17, 18], these particles are carbides formed due to the small amount of carbon in the 316L SS and the slight carbon contaminations from the graphite cathode. Figure 4(b) gives the selected area electron diffraction (SAED) pattern corresponding to Figure 4(a). Clearly, this pattern comes from the diffraction of a single crystal without large misorientations, suggesting that all the cells observed in Figure 4(a) have nearly the same crystallographic orientation. This is in consistency with the EBSD analysis (Figure 3) that the grains are actually not significantly refined after the direct HCPEB treatment. The TEM observations were also carried out in the surface layer of the Ti alloyed sample. Figure 5(a) shows a typical bright field TEM image of the Ti alloyed sample. It reveals fine grains having size from 80 to 200 nm formed in the surface layer. These grains show different contrasts, suggesting that they have different orientations. A typical dark field image with the α phase grains in bright contrast is given in Figure 5(b). It confirms the formation of nanosized α phase grains. The corresponding SAED pattern given in the inset of Figure 5(b) is composed of many diffraction rings, indicating that those nanograins have spread orientations. These diffraction rings can be indexed with either α phase or γ phase, which is consistent with the XRD analyses (Figure 2(b)).

3.3. Discussions. When the pulsed electron beam irradiates on the surface of a target material, the kinetic energy of electron beam is transferred into heat immediately through interactions of the beam with atoms in the surface layer [2, 6]. The transient thermal energy induces fast heating, melting, and possible evaporating followed by the resolidification and cooling [9–12]. In the case of the direct HCPEB treated 316L SS sample, the surface is melted by the electron beam and solidifies later on the substrate below the melted layer. Since no new phase but austenite forms in the melted layer, an epitaxial type growth is preferred due to the low melt-substrate interface energy. As a result, the grain size is very close to that in the substrate. However, the moving speed of solid-liquid interface is extremely high during solidification, typically around several meters per second as calculated through numerical simulations [19, 20]. Thus the interface may not be stable anymore and may have a cell-like morphology [21]. Those small carbide particles or segregates will be pushed out from the newly formed solid phase and stay at the cell boundaries. For the Ti alloyed sample, the melting and solidification are very different from those taking place on the direct HCPEB treated sample. First, the thick Ti powder layer becomes thinner due to the electron beam sputtering and is melted with the substrate underneath. Then, Ti is dissolved into the steel substrate through liquid state mixing [22]. During the solidification, the Ti rich areas will solidify to form α phase while Ti lean areas keep the γ phase as the primary solidification phase. Under such a condition, epitaxial growth is not preferred during solidification as two phases nucleate from the melt simultaneously. Due to the very high cooling rate in the melt, the nucleation rate can be very high, leading to the significant refining of the surface alloyed layer [23, 24]. The formation of such alloyed layer with two-phase nanostructures is proved to improve significantly the corrosion resistance of the 316L SS [22].

4. Conclusions

This work has examined the formation of nanostructures in the AISI 316L stainless steel induced by HCPEB treatments. It is shown that a two-phase nanostructure containing α and γ phases can form on the HCPEB Ti alloyed sample. In comparison, a pseudo nanostructure having γ phase cells in nanoscale but without misorientations formed on the direct HCPEB treatment. Therefore, the rapid solidification itself may not ensure the significant refinement of microstructures on the HCPEB treated material. New phases other than the substrate should nucleate in the melted layer so that real nanostructured layer can be generated on the HCPEB treated sample surface.

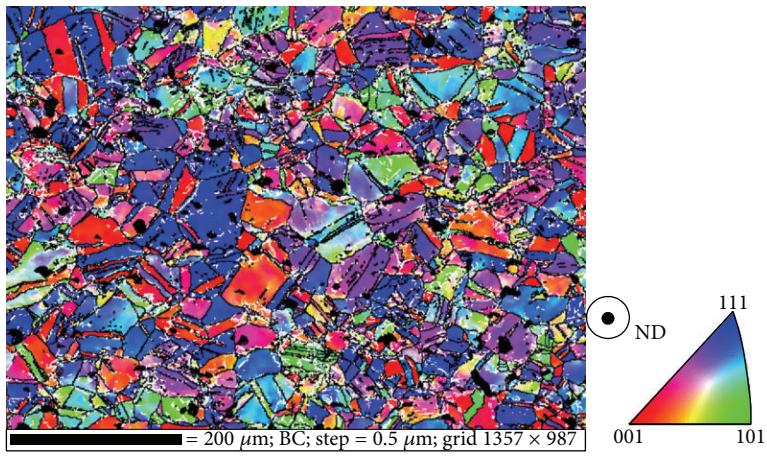

Figure 3: EBSD orientation map taken on the direct HCPEB treated sample.

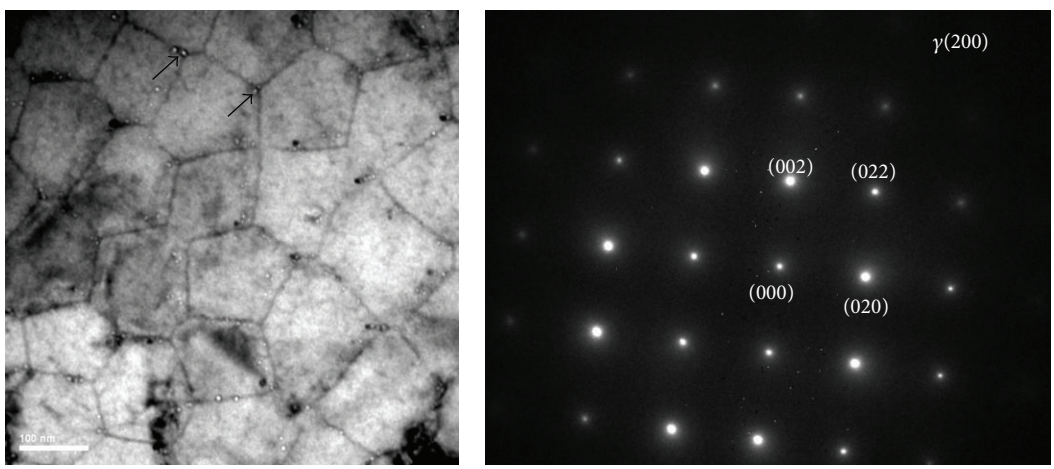

(a) (b)

Figure 4: Typical TEM bright field image (a) of the surface layer of the direct HCPEB treated sample and the corresponding SAED pattern (b).

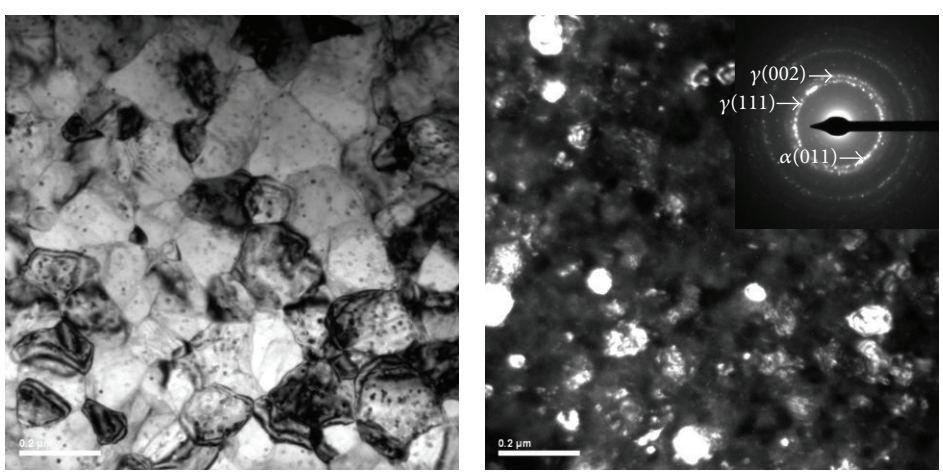

(a) (b)

Figure 5: Typical TEM bright field image (a) and dark field image (b) of the surface layer of the Ti alloyed sample and the corresponding SAED pattern of (b) are shown in inset.

Conflict of Interests

The authors declare that there is no conflict of interests regarding the publication of this paper.

Acknowledgments

Professor Kemin Zhang would like to acknowledge Shanghai University of Engineering Science Innovation Fund for Graduate Students (no. 13KY0501) and Shanghai Innovation Fund for Undergraduate Students (no. cs 1305005). This work is supported by the National Natural Science Foundation (nos. 51101096, 51271121).

References

[1] M. Sorescu, "The role of magnetostriction in pulsed laser irradiation of amorphous alloys," *Journal of Alloys and Compounds*, vol. 280, no. 1-2, pp. 251–254, 1998.

[2] D. I. Proskurovsky, V. P. Rotshtein, G. E. Ozur et al., "Pulsed electron-beam technology for surface modification of metallic materials," *Journal of Vacuum Science and Technology A: Vacuum, Surfaces and Films*, vol. 16, no. 4, pp. 2480–2488, 1998.

[3] X. Y. Le, S. Yan, W. J. Zhao, B. X. Han, Y. G. Wang, and J. M. Xue, "Computer simulation of thermal-mechanical effects of high intensity pulsed ion beams on a metal surface," *Surface and Coatings Technology*, vol. 128-129, no. 1, pp. 381–386, 2000.

[4] V. Engelko, G. Mueller, A. Rusanov et al., "Surface modification/alloying using intense pulsed electron beam as a tool for improving the corrosion resistance of steels exposed to heavy liquid metals," *Journal of Nuclear Materials*, vol. 415, no. 3, pp. 270–275, 2011.

[5] D. I. Proskurovsky, V. P. Rotshtein, G. E. Ozur, Y. F. Ivanov, and A. B. Markov, "Physical foundations for surface treatment of materials with low energy, high current electron beams," *Surface and Coatings Technology*, vol. 125, no. 1–3, pp. 49–56, 2000.

[6] C. Dong, A. M. Wu, S. Z. Hao et al., "Surface treatment by high current pulsed electron beam," *Surface and Coatings Technology*, vol. 163-164, pp. 620–624, 2003.

[7] Y.-K. Gao, "Influence of pulsed electron beam treatment on microstructure and properties of TA15 titanium alloy," *Applied Surface Science*, vol. 264, pp. 633–635, 2013.

[8] X. D. Zhang, S. Z. Hao, X. N. Li, C. Dong, and T. Grosdidier, "Surface modification of pure titanium by pulsed electron beam," *Applied Surface Science*, vol. 257, no. 13, pp. 5899–5902, 2011.

[9] J. X. Zou, T. Grosdidier, K. M. Zhang, and C. Dong, "Mechanisms of nanostructure and metastable phase formations in the surface melted layers of a HCPEB-treated D2 steel," *Acta Materialia*, vol. 54, no. 20, pp. 5409–5419, 2006.

[10] J. W. Murray, J. C. Walker, and A. T. Clare, "Nanostructures in austenitic steel after EDM and pulsed electron beam irradiation," *Surface and Coatings Technology*, vol. 259, pp. 465–472, 2014.

[11] J. Kim, S. S. Park, and H. W. Park, "Corrosion inhibition and surface hardening of KP1 and KP4 mold steels using pulsed electron beam treatment," *Corrosion Science*, vol. 89, pp. 179–188, 2014.

[12] J. Cai, S. Z. Yang, L. Ji, Q. F. Guan, Z. P. Wang, and Z. Y. Han, "Surface microstructure and high temperature oxidation resistance of thermal sprayed CoCrAlY coating irradiated by high current pulsed electron beam," *Surface and Coatings Technology*, vol. 251, pp. 217–225, 2014.

[13] V. P. Rotshtein, Y. F. Ivanov, Y. A. Kolubaeva et al., "Synthesis of Ti_3Al and TiAl based surface alloys by pulsed electron-beam melting of Al(film)/Ti(substrate) system," *Technical Physics Letters*, vol. 37, pp. 226–229, 2011.

[14] J. X. Zou, K. M. Zhang, C. Dong, Y. Qin, S. Hao, and T. Grosdidier, "Selective surface purification via crater eruption under pulsed electron beam irradiation," *Applied Physics Letters*, vol. 89, no. 4, Article ID 041913, 2006.

[15] Y. Qin, C. Dong, Z. F. Song et al., "Deep modification of materials by thermal stress wave generated by irradiation of high-current pulsed electron beams," *Journal of Vacuum Science & Technology A*, vol. 27, no. 3, pp. 430–435, 2009.

[16] T. B. Massalski, *Binary Alloy Phases Diagrams*, ASM International, Materials Park, Ohio, USA, 1990.

[17] V. P. Rotshtein, D. I. Proskurovsky, G. E. Ozur, Y. F. Ivanov, and A. B. Markov, "Surface modification and alloying of metallic materials with low-energy high-current electron beams," *Surface and Coatings Technology*, vol. 180-181, pp. 377–381, 2004.

[18] Y. Ivanov, W. Matz, V. Rotshtein, R. Günzel, and N. Shevchenko, "Pulsed electron-beam melting of high-speed steel: structural phase transformations and wear resistance," *Surface and Coatings Technology*, vol. 150, no. 2-3, pp. 188–198, 2002.

[19] J. X. Zou, K. M. Zhang, T. Grosdidier, and C. Dong, "Analysis of the evaporation and re-condensation processes induced by pulsed beam treatments," *International Journal of Heat and Mass Transfer*, vol. 64, pp. 1172–1182, 2013.

[20] J. Zou, Y. Qin, C. Dong, X. Wang, A. Wu, and S. Hao, "Numerical simulation of the thermal-mechanical process of high current pulsed electron beam treatment," *Journal of Vacuum Science & Technology A*, vol. 22, no. 3, pp. 545–552, 2004.

[21] W. J. Boettinger, S. R. Coriell, A. L. Greer et al., "Solidification microstructures: recent developments, future directions," *Acta Materialia*, vol. 48, no. 1, pp. 43–70, 2000.

[22] K. M. Zhang, J. X. Zou, T. Grosdidier, C. Dong, and S. Weber, "Ti surface alloying of an AISI 316L stainless steel by low energy high current pulsed electron beam treatment," *Journal of Vacuum Science & Technology A*, vol. 26, no. 6, pp. 1407–1414, 2008.

[23] B. Gao, Y. Hao, G. F. Tu et al., "Surface modification of Mg_{67}-Zn_{30}-Y_3 quasicrystal alloy by high current pulsed electron beam," *Surface and Coatings Technology*, vol. 229, pp. 42–45, 2013.

[24] B. Gao, J. He, G. F. Tu, and L. Hu, "Nanocrystallization of coarse primary phases in Al- and Mg-based alloys induced by HCPEB treatment," *Journal of Nanomaterials*, vol. 2013, Article ID 815384, 6 pages, 2013.

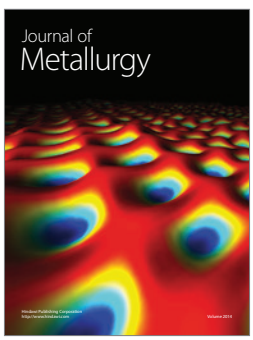

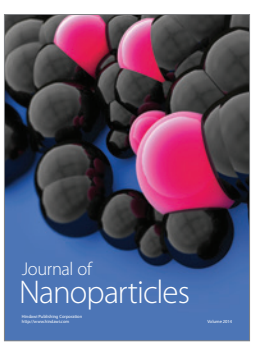

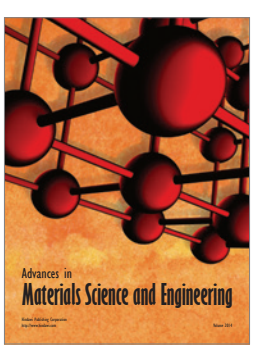

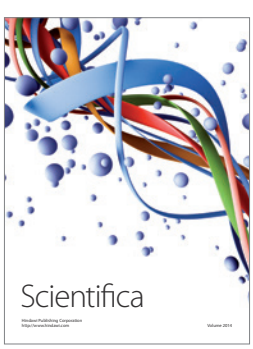

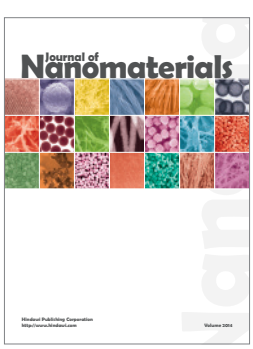

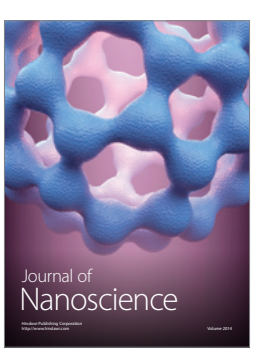

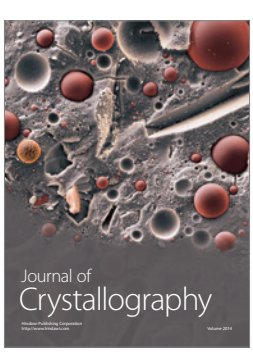

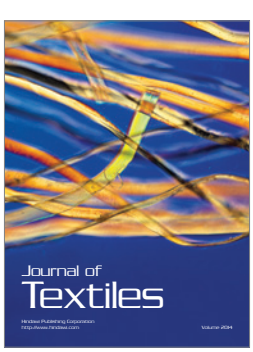

Hindawi

Submit your manuscripts at
http://www.hindawi.com